Published in final edited form as:
Biochemistry. 2010 August 24; 49(33): 7227–7237. doi:10.1021/bi100805b.

Structural Analysis of WbpE from *Pseudomonas aeruginosa* PAO1: A Nucleotide Sugar Aminotransferase Involved in O-antigen Assembly†

Angelyn Larkin‡, **Nelson B. Olivier**‡, and **Barbara Imperiali**‡,§,*

‡ Department of Chemistry, Massachusetts Institute of Technology, 77 Massachusetts Avenue, Cambridge, MA 02139

§ Department of Biology, Massachusetts Institute of Technology, 77 Massachusetts Avenue, Cambridge, MA 02139

Abstract

In recent years, the opportunistic pathogen *Pseudomonas aeruginosa* has emerged as a major source of hospital-acquired infections. Effective treatment has proven increasingly difficult due to the spread of multidrug resistant strains and thus requires a deeper understanding of the biochemical mechanisms of pathogenicity. The central carbohydrate of the *P. aeruginosa* PAO1 (O5) B-band O-antigen, ManNAc(3NAc)A, has been shown to be critical for virulence and is produced in a stepwise manner by five enzymes in the Wbp pathway (WbpA, WbpB, WbpE, WbpD and WbpI). Herein, we present the crystal structure of the aminotransferase WbpE from *P. aeruginosa* PAO1 in complex with the cofactor pyridoxal 5′-phosphate (PLP) and product UDP-GlcNAc($3NH_2$)A as the external aldimine at 1.9 Å resolution. We also report the structures of WbpE in complex with PMP alone as well as the PLP internal aldimine, and show that the dimeric structure of WbpE observed in the crystal structure is confirmed by analytical ultracentrifugation. Analysis of these structures reveals that the active site of the enzyme is composed of residues from both subunits. In particular, we show that a key residue (Arg229), which has previously been implicated in direct interactions with the carboxylate moiety of α-ketoglutarate, is also uniquely positioned to bestow specificity for the 6″ carboxyl group of GlcNAc($3NH_2$)A through a salt bridge. This finding is intriguing, because while an analogous basic residue is present in WbpE homologs that do not process C6″-carboxyl-modified saccharides, recent structural studies reveal that this side chain is retracted to accommodate a neutral C-6″ carbon. This work represents the first structural analysis of a nucleotide sugar aminotransferase with a bound product modified at the C2″, C3″, and C6″ positions and provides insight into a novel target for treatment of *P. aeruginosa* infection.

Pseudomonas aeruginosa is a Gram-negative pathogen responsible for severe infection in immunocompromised individuals. In recent years, it has emerged as a major source of hospital-acquired infections, such as bacteremia, pneumonia and febrile neutropenia, and leads to inflammation and pulmonary failure in cystic fibrosis patients (1–5). While there are several standard antibiotics currently used to combat *P. aeruginosa*, the rapidly increasing

†This work was supported by a grant from National Institutes of Health (GM039334 to B.I.).

*To whom correspondence should be addressed: Massachusetts Institute of Technology, 77 Massachusetts Avenue, Cambridge, MA 02139. Phone: (617) 253-1838; Fax: (617) 452-2419; imper@mit.edu.

SUPPORTING INFORMATION AVAILABLE

Sedimentation velocity analytical ultracentrifugation data, analysis of WbpE alanine mutants and the His308-Tyr309 *cis* amide bond, as well as a sequence alignment of WbpE homologs from pathogenic bacteria. This material is available free of charge via the Internet at http://pubs.acs.org.

occurrence of multidrug resistant strains has complicated treatment and highlighted the need for alternative drug design strategies (6–8). One of the most promising targets for improved treatment is the bacterial lipopolysaccharide (LPS)1, found in the exterior leaflet of the outer membrane of the organism. The LPS of *P. aeruginosa* contains the B-band O-antigen unit, a critical virulence factor that has been shown to play a key role in host colonization and evasion of immune defenses (9–11). Genetic mutants of *P. aeruginosa* deficient in B-band O-antigen have exhibited greatly increased sensitivity to phagocytosis and serum-mediated killing (12).

The B-band O-antigen of *P. aeruginosa* PAO1 (serotype O5) is composed of repeating units of a trisaccharide made up of 2-acetamido-3-acetamidino-2,3-dideoxy-*β*-D-mannuronic acid (ManNAc(3NAm)A), 2,3-diacetamido-2,3-*β*-D-mannuronic acid (ManNAc(3NAc)A), and *N*-acetyl-*α*-D-fucosamine (Fuc2NAc) (13). Recent studies have shown that the central saccharide unit, ManNAc(3NAc)A, is synthesized by five enzymes in the Wbp pathway (WbpA, B, E, D, and I) starting from the common precursor, UDP-GlcNAc (Figure 1) (14). In the first step, WbpA oxidizes the C6″ hydroxyl group to afford UDP-GlcNAcA. This is followed by the coupled action of the dehydrogenase WbpB and aminotransferase WbpE to yield UDP-GlcNAc($3NH_2$)A through a unique NAD^+ recycling pathway (15). Finally, the acetyltransferase WbpD and epimerase WbpI provide the final UDP-ManNAc(3NAc)A donor, which is then transferred to an undecaprenyl carrier. After completion, the trisaccharide is flipped into the bacterial periplasm by the Wzx translocase and then ligated to the growing O-antigen by Wzy polymerase (16).

WbpE is a pyridoxal 5′-phosphate (PLP)-dependent aminotransferse responsible for the conversion of UDP-GlcNAc(3keto)A and L-glutamate to UDP-GlcNAc($3NH_2$)A and *α*-ketoglutarate (*α*-KG), respectively. It is a member of the broad class of Fold Type I aspartate-aminotransferase (AAT) enzymes, which harness the powerful electron-sink properties of PLP to carry out a wide variety of transformations, including transaminations, eliminations, decarboxylations, and racemizations (17,18). The general mechanism of this class of enzymes has been worked out in great detail, and is divided into two discrete half reactions that cycle between the PMP and PLP forms of the cofactor (Figure 2). The reaction begins with imine formation between the ketone-bearing sugar and PMP, followed by abstraction of a C4′ proton of PMP by the catalytic lysine residue of the protein. The resulting quinoid intermediate then accepts a proton from the lysine at the C3″ carbon of the pyranose, which serves to set the stereochemistry at this position and results in the external aldimine intermediate. Release of the nucleotide sugar amine product is facilitated by transimination to afford the internal aldimine. In the second half of the catalytic cycle, the reaction steps are repeated in the reverse order resulting in regeneration of PMP through conversion of L-glutamate to *α*-ketoglutarate.

In this report, we present the crystal structure of the aminotransferase WbpE from *P. aeruginosa* PAO1 in complex with three different ligands: PMP, PLP, and the external aldimine of PLP with the reaction product, UDP-GlcNAc($3NH_2$)A. In recent years, the crystal structures of several Fold Type I enzymes that catalyze the transamination of nucleotide sugars in bacteria have been described (19–24). These studies have revealed that

[1]Abbreviations: AAT, aspartate aminotransferase; Bis-Tris, 2-Bis-(2-hydroxyethyl)amino-2-(hydroxymethyl)-1,3-propanediol; CE, capillary electrophoresis; DTT, dithiothreitol; EDTA, ethylenediaminetetraacetic acid; HEPES, 4-(2-hydroxyethyl)-1-piperazineethanesulfonic acid; IPTG, isopropyl *β*-D-1-thiogalactopyranoside; *α*-KG, *α*-ketoglutarate; LPS, lipopolysaccharide; Ni-NTA, nickel nitrilotriacetic acid; PLP, pyridoxal 5′-phosphate; PMP, pyridoxamine 5′-phosphate; r.m.s.d, root mean square deviation; RP-HPLC, reversed-phase high-performance liquid chromatography; TEAB, triethylammonium bicarbonate; TEV, tobacco etch protease; UDP, uridine 5′-diphosphate; UDP-GlcNAc, UDP-*N*-acetyl-D-glucosamine; UDP-GlcNAcA, UDP-*N*-acetyl-D-glucosaminuronic acid; UDP-GlcNAc(3keto)A, UDP-2-acetamido-2-deoxy-3-oxo-D-glucuronic acid; UDP-GlcNAc($3NH_2$)A, UDP-2-acetamido-3-amino-2,3-dideoxy-D-glucuronic acid; UDP-ManNAc(3NAc)A, UDP-2,3-diacetamido-2,3-dideoxy-D-mannuronic acid.

while members of this enzyme class share many similarities in the cofactor-binding site, the factors that govern binding and specificity of the nucleotide sugar substrates are not yet fully understood. This work presents the first structure of an aminotransferase that binds a nucleotide sugar modified at the C2″, C3″ and C6″ positions, and thus provides a glimpse into the means by which such a highly functionalized nucleotide sugar is accommodated in the enzyme active site. In addition, we confirm that WbpE associates as a homodimer in solution using sedimentation velocity analytical ultracentrifugation. In order to gain a broader understanding of nucleotide sugar specificity across this class of aminotransferases, we compare our WbpE structure in complex with the external aldimine to the other nucleotide sugar-bound aminotransferase structures. We envision that this work will add to the growing body of knowledge about nucleotide sugar aminotransferases and may also present a novel target for the development of antimicrobial treatments to combat *P. aeruginosa*.

EXPERIMENTAL PROCEDURES

Molecular Biology

The *wbpE* gene was amplified from *Pseudomonas aeruginosa* PAO1-LAC genomic DNA (ATCC) by the polymerase chain reaction as previously described, using primers to introduce 5′ *Bam*HI and 3′ *Xho*I restriction sites (15). The resulting oligonucleotide was then inserted into a modified pET32a vector (Novagen) using standard molecular biology techniques. Site-directed mutagenesis was performed using the QuikChange protocol from Stratagene with the *wbpE*-pET32a plasmid as a template. All constructs yielded proteins with an N-terminal His_6-tag followed by a tobacco etch protease (TEV) site for tag removal.

Overexpression of WbpE

The *wbpE*-pET32a plasmid was transformed into *E. coli* BL21-CodonPlus(DE3) RIL competent cells (Stratagene) for heterologous expression, using both kanamycin (50 μg/mL) and chloramphenicol (30 μg/mL) for selection. The cell culture was grown to an optical density (600 nm) of 0.8–1.0 at 37 °C in Luria-Bertani broth; the culture was subsequently cooled to 16 °C and protein expression was induced through the addition of IPTG (1mM). After 16 h, the cells were harvested by centrifugation (5000*g*) and the resulting cell pellets were stored at −80 °C for future use. Incorporation of selenomethionine was accomplished using the method of metabolic inhibition described elsewhere with slight modification (25). Briefly, 0.5 L of M9 medium supplemented with 1 mM $MgSO_4$, 3 mM $FeSO_4$, 0.4% (w/v) glucose, 0.5% (w/v) thiamine, kanamycin (50 μg/mL) and chloramphenicol (30 μg/mL) was inoculated with 5 mL starter culture and allowed to incubate at 37 °C until the desired optical density (0.8–1.0) was obtained. Prior to induction, the following amino acids were added to the flask and the culture was incubated for 15 minutes to allow for the inhibition of methionine biosynthesis: L-lysine (100 mg/L), L-phenylalanine (100 mg/L), L-threonine (100 mg/L), L-isoleucine (50 mg/L), L-leucine (50 mg/L), L-valine (50 mg/L), L-selenomethionine (60 mg/L). After addition of IPTG (1 mM) to induce protein expression, the culture was handled as described above.

Purification of WbpE

All steps were performed at 4 °C. WbpE was purified from cell pellets using Ni-NTA resin (Qiagen) as previously described (15). After overnight dialysis to remove the imidazole and lower the salt concentration, the N-terminal His_6-tag was removed by proteolysis with TEV over the course of three days while stirring in dialysis buffer (50 mM HEPES, pH 8.0/100 mM NaCl/4% glycerol/0.5 mM EDTA/5 mM DTT); the removal of the tag was confirmed by Western blot analysis using an Anti-His_4 anitbody (Qiagen). The protein was then subjected to size-exclusion chromatography using a Superdex 200 16/60 column (GE

Healthcare) in running buffer composed of 25 mM HEPES, pH 8.0/100 mM NaCl/0.5% glycerol. Fractions containing monodispersed protein were pooled and analyzed by SDS-PAGE for purity and MALDI mass spectrometry to quantify selenomethionine incorporation. Purified protein was routinely utilized within 24 h to prevent aggregation.

Sedimentation Velocity Analytical Ultracentrifugation

Experiments were conducted in an Optima XL-I ultracentrifuge (Beckman Coulter) using an An60 Ti rotor at 4 °C with a rotor speed of 42,000 rpm. Data were acquired by monitoring absorbance at 280 nm through quartz cell windows. A sample of WbpE (36 μM) was dialyzed against 25 mM HEPES, pH 8.0/100 mM NaCl/0.5% glycerol for 24 h prior to the experiment; the centrifugation run also included dialysis buffer as a blank. Data were analyzed with the software package SEDNANAL (26) to determine the oligomeric state of the protein in solution.

Synthesis of UDP-GlcNAc(3NH$_2$)A

The UDP-GlcNAc(3NH$_2$)A product of WbpE was prepared starting from UDP-GlcNAcA using the coupled enzyme reaction of WbpB and WbpE as previously described with slight modification (15). UDP-GlcNAcA (0.75 mM), NAD^+ (0.2 mM), L-glutamate (25 mM), PLP (0.1 mM), DTT (2.5 mM) and $MgCl_2$ (2 mM) were combined in 50 mL of HEPES buffer (50 mM, pH 8.0) with 4.5 mg each of WbpB and WbpE and incubated for 10 h at 30 °C. After filtration to remove protein, the crude reaction mixture was purified using a Synergi C_{18} Hydro preparatory RP-HPLC column (4 μm, 80 Å, 250 × 21.2 mm, Phenomenex) equilibrated with 50 mM TEAB (pH 7.1); the desired product was eluted with a linear gradient of 0–50% CH_3CN over 85 minutes. In order to remove the TEAB salt for crystallization, UDP-GlcNAc(3NH$_2$)A was dissolved in distilled, deionized water and subjected to cation exchange chromatography using a 1 mL HiTrap SP FF column (GE Healthcare).

Crystallization and Data Collection

Prior to setting up crystal trays, WbpE was concentrated to 10 mg/mL in the size-exclusion running buffer. For crystallization in the presence of ligands, PLP and/or UDP-GlcNAc(3NH$_2$)A were added to the protein solution at a final concentration of 500 μM and 10 mM respectively and allowed to incubate on ice for 1 h. Crystals were obtained at 25 °C from a hanging drop by mixing 1.5 μL protein solution with 1.5 μL reservoir solution. All crystals except for the SeMet derivative were grown in a reservoir solution containing 0.1 M Bis-Tris, pH 5.5, 0.2 M ammonium sulfate and 25% PEG 3350. SeMet crystals were grown in a reservoir solution containing 0.1 M Bis-Tris, pH 5.5, 0.2 M ammonium acetate, 10 mM $SrCl_2$ and 25% PEG 3350. Crystals were cryoprotected in the corresponding reservoir solution supplemented with 20% glycerol and substrate as necessary. Diffraction data were collected on beamline X6A (National Synchrotron Light Source, Brookhaven National Laboratory, Upton, NY) at 110 K. For the SeMet derivative, data were collected at the selenium peak (12667 eV), edge (12660 eV) and remote (12867 eV). Data sets were indexed and scaled using HKL2000 (27), and the scaled intensities were converted to structure factors using the program TRUNCATE in the CCP4 suite of programs (28). Data collection parameters are summarized in Table 1.

Structure Determination and Refinement

The structure of the WbpE-SeMet derivative was solved using the method of multiwavelength anomalous diffraction (29). Using data collected at the selenium peak and truncated to 2.5 Å, the program SOLVE (30) was employed to locate the heavy atom sites and generate experimental phases. A total of four out of five selenium atoms were located

for each protein subunit. The initial model was built using the prime-and-switch phasing feature of RESOLVE (31,32) to minimize model bias and contained the basic framework of the model, except for sizeable gaps between residues 116–142 and 196–233. The PMP-bound structure was then solved by molecular replacement using Phaser (33) with the SeMet derivative as the initial search model. Further model building and refinement were carried out using Coot (34) and Refmac (35). Five percent of the data were used to calculate the R_{free} values for cross-validation of the refinement process (36). The structures of the PLP and external aldimine complexes were subsequently solved by molecular replacement in the same manner, using the completed PMP-bound structure with the cofactor removed as the input model. Water molecules were added using both ARP/wARP (37) and Coot, and ligands were modeled into each structure after the R_{free} value was below 30%. All refined structures were validated using PROCHECK (38), SFCHECK (39) and MolProbity (40), and the final refinement statistics are presented in Table 1. All molecular images were generated using PyMOL.

Functional Characterization of WbpE Alanine Mutants

Enzyme mutants were analyzed for function using the coupled WbpB/WbpE assay slightly modified from that described elsewhere (15). In brief, 2.5 μg of each WbpE mutant was incubated with UDP-GlcNAcA (0.75 mM), NAD^+ (0.2 mM), L-glutamate (25 mM), PLP (0.1 mM), DTT (2.5 mM), $MgCl_2$ (2 mM) and 2.5 μg of WbpB in 60 μL of 50 mM HEPES buffer (pH 8.0) for 2 h at 30 °C. Capillary electrophoresis (P/ACE MDQ System, Beckman Coulter) was used to monitor enzyme activity as outlined previously, and the presence of product was confirmed by the addition of starting material into the reaction mixtures and the observation of a new peak on the CE chromatogram.

RESULTS

Overall Architecture of WbpE

WbpE crystallized in the orthorhombic space group $P2_12_12$, with two molecules in the asymmetric unit and approximate unit cell dimensions of 75 Å × 150 Å × 50 Å (Figure 3). The overall scaffold of WbpE is similar to that of other members in the Fold Type 1 aminotransferase family, with aspartate aminotransferase (AAT) representing the first and most well-studied member (41,42). As in the case of AAT, each monomer of WbpE can be divided into two major domains: a large N-terminal PLP-binding region and a smaller C-terminal domain (Figure 3c). The N-terminal portion (residues Ile14-Glu243) is composed of a total of eleven β-strands, seven of which make up a central β-sheet that exhibits the canonical strand order β-1, β-9, β-8, β-5, β-4, β-2, β-3, where β-9 is antiparallel to the others. This β-sheet is bordered on the top and bottom faces by seven α-helices. After strand β-9, a short stretch of residues (Gln209-Arg229) extends out from the monomer structure to form a large domain-swapped β-hairpin (β-10 and β-11) that interacts with the active site of other monomer. Another smaller β-hairpin (residues Ala163-Ser170, β-6 and β-7) protrudes from the top face of the central β-sheet and interacts with the C-terminal region in the same subunit. The C-terminal portion of the protein (residues Met1-Arg13, Ile244-Asn359) is made up of two short β-strands and six α-helices that are oriented away from each other in a V-shape. The entire C-terminal region of the protein is closely aligned to the N-terminal domain on the top face of the monomer, yet opens to reveal a deep channel on the opposite face of the subunit, allowing solvent access to the enzyme active site (Figure 3b). In addition, this domain of the protein contains a non-prolyl *cis* amide bond between residues His308 and Tyr309.

The interface between the subunits of the dimer is extensive and comprises an area of approximately 7500 $Å^2$, which represents nearly 25% of the total surface area of a single

subunit. The two active sites of the dimer are open to one another and are spaced roughly 30 Å apart. The most striking interaction between the two monomers is the presence of the domain-swapped β-hairpin that crosses over the dimer interface and lines the entrance to the active site tunnel of the neighboring subunit. Other notable interactions between the monomers include the stacking of two homologous antiparallel α-helices from each monomer, both comprising residues Ile14-His28, as well as the loop residues Cys189-Gly193 from one subunit that nestle beneath residues Gly29-Leu33 from the other (Figure 3).

Sedimentation velocity analytical ultracentrifugation studies were undertaken in order to establish whether the dimerization of WbpE observed in the crystal structure correlates with the oligomeric state present in solution. The sedimentation coefficient was found to be 4.72 Svedberg units and the molecular mass was calculated as 79.3 kD using a single species model fit. As each monomer of WbpE has a theoretical molecular weight of 38.9 kD, the data suggest that WbpE associates as a dimer in solution (Figure S1, Supporting Information). This finding is in keeping with other members of the Fold Type 1 aminotransferase family, which have been found to exist primarily as homodimers or other higher-order oligomers in mutiples of two (18).

The Cofactor-Binding Site

During structure refinement, both the SeMet derivative and native form of WbpE were discovered to contain the cofactor bound to the enzyme active site despite the fact that it was not exogenously introduced over the course of protein expression or purification. The electron density of the cofactor was unambiguous and thus modeled into the native structure at full occupancy (Figure 4). It was determined that the cofactor was present in the PMP form due to the retracted position of the catalytic lysine residue (Lys185) as well as the lack of electron density between the C4′ carbon of the cofactor and the lysine nitrogen atom, indicating that there was no covalent bond present. In addition, the UV spectrum of purified WbpE possessed the spectral characteristics of PMP, namely the presence of an absorbance maximum at 340 nm compared with that at 420 nm indicative of PLP (data not shown). In order to obtain the PLP-bound form of the enzyme (internal aldimine), PLP was incubated with WbpE for 1 h prior to setting up crystal trays. In contrast to the PMP-bound crystals, the PLP-bound structure showed an extended conformation of Lys185 and clear electron density between the side chain and the cofactor, serving as evidence that the cofactor was held in place by a covalent bond (Figure 4).

The cofactor-binding site resides within a deep cleft in the interior of each monomer at the far end of the joined active sites. The cofactor is oriented such that the pyridinium ring is facing inward, resting above the central β-sheet of each monomer unit, while the phosphate moiety points toward the entrance of the cleft and is located 20 Å from the phosphate group in the other subunit. The pyridinium ring is flanked on the top face by Tyr85, with which it is interacting in a π-π stacking fashion, and the bottom face by Ala158. The C5′ hydroxyl group of the cofactor is within hydrogen-bonding distance of Gln159 and Tyr309, while the C6′ methyl group is in close proximity (3.3 Å) to Val130. The N1 nitrogen of the pyridinium ring is held in place by a salt bridge with the carboxylate of Asp156 that serves to enhance the electron-sink properties of the cofactor. This aspartate residue is conserved in all Fold Type I aminotransferases and is crucial for maintaining the cofactor in its protonated state (17). In the PMP-bound form of the enzyme, the C4′ amine does not appear to interact with any specific residues, as the closest atom is the oxygen of a water molecule more than 4 Å away. Examination of a space-filling model of the PMP-bound form of WbpE shows that the C4′ amine lies at the bottom of the deep solvent tunnel leading to the outside of the active site, making it accessible for reaction with incoming substrate (Figure 3b). The phosphate group of the cofactor protrudes into the entrance to the active site in the opposite direction

and is held in place by several hydrogen-bonding and charge stabilizing interactions, including those with Ser180, Thr60, Gly59, Asn227 of the β-hairpin from the other subunit and three well-ordered water molecules.

An analysis of the residues surrounding the cofactor in both the PMP and PLP-bound structures indicate that there is very little conformational change in the overall architecture of WbpE upon formation of the internal aldimine (Figure 4); the root mean square deviation of these two structures is 0.32 Å. Differences include the slight upward shift of the pyridinium ring into the active site due to the presence of the imine bond as well as small changes in the orientation of the Tyr85 side chain. In addition, the domain-swapped β-hairpin stretches closer toward the active site in the PLP-bound structure; slight changes can be seen in the side chain orientations of Gln215 and Arg212 that reflect this movement.

The Nucleotide Sugar-Binding Site

Crystals of WbpE complexed with the external aldimine were obtained by incubating the enzyme with both PLP and the UDP-GlcNAc(3NH_2)A product on ice for 1 h prior to crystallization. The presence of the external aldimine in the enzyme active site implies that the reaction proceeded in reverse upon exposure to the aminated product; this intermediate was previously observed in other nucleotide sugar-bound aminotransferase structures as well (20,22,24). The external aldimine is bound in both subunits of the dimer, and electron density between the pyridinium C4′ carbon and the C3″ position of the hexose ring indicates the existence of a covalent bond (Figure 5a). As in the case of the WbpE complexes with PMP and PLP, the electron density for the cofactor portion of the ligand is very strong; however, the density for the nucleotide sugar component is weaker, with an average temperature factor <*B*> of 42.8 $Å^2$ compared with that for the cofactor (26.8 $Å^2$) and nearby protein atoms (21.6 $Å^2$). The weakest regions of electron density in the external aldimine structure are surrounding the C4″ hexose carbon as well as the C2′ and C3′ carbon bond in the ribose moiety. This observation suggests that the nucleotide sugar region of the aldimine is not as firmly held in place as the cofactor and may experience some thermal motion within the crystal. For this reason, atoms comprising the nucleotide sugar were refined at 50% occupancy.

The glucopyranose ring of the ligand is bound to the cofactor through the C3″ carbon and, as depicted in Figure 5, many interactions take place between this highly functionalized sugar and the protein to accommodate it within the active site. The aromatic side chains of Tyr85 and Phe182 are stacked above and below the glucopyranose ring, presumably forming a barrier to prevent solvent access throughout the course of catalysis. In addition, these residues may serve to stabilize the positively charged reaction intermediates through cation-π interactions. The C2″ acetamido oxygen participates in hydrogen bonds with both the side chain phenol of Tyr309 as well as the C5′ hydroxyl group of the cofactor pyridinium ring, while the C4″ hydroxyl is within hydrogen-bonding distance of the cofactor phosphoryl group. The C6″ carboxylate is coordinated to a well-ordered water molecule that is hydrogen-bonded to both the phosphate group and the imidazole ring of His213, which is part of the domain-swapped β-hairpin from the neighboring protein subunit. In addition to this water molecule, the carboxylate is held in place by a salt bridge with the guanidinium moiety of Arg229, also from the β-hairpin domain. This arginine residue is commonly found in Fold Type 1 aminotransferases and is believed to play a critical role in binding L-glutamate and α-KG during the course of the reaction (18).

The pyrophosphate of the nucleotide sugar extends away from the glucopyranose through the deep protein cavity that leads to the exterior of the protein, and is anchored by interactions with Ser184, His308 and at least two well-ordered waters. The uridine emerges from this channel and is fully exposed to the solvent, making van der Waals contacts with

one α-helix from each of the dimer subunits and residues from both monomer units on the bottom face and several water molecules from above. The ribose 3′-OH group participates in hydrogen bonds with the N-terminal region of the protein, including the side chain of Glu3 and the backbone carbonyl of Ile5, while the uracil is in close proximity to numerous residues in the neighboring subunit, including Gly29, Tyr31 and Ile32.

Comparison of the WbpE complexes with PMP and the external aldimine reveals that as in the case with the internal aldimine structure, no major conformational change is observed in the overall architecture of the protein upon substrate binding. Analysis of the overlaid cofactor and external aldimine-bound structures indicates only small differences between the two forms of the enzyme (r.m.s.d. = 0.33 Å), with the most notable changes within the domain-swapped β-hairpin shifting slightly around the enzyme active site.

Analysis of WbpE Alanine Mutants

Comparison of the cofactor- and nucleotide sugar-bound structures of WbpE led to the identification of eight key amino acid residues that appear to play a critical role in substrate binding. These residues are found in both subunits of the dimer and contact the cofactor and/or substrate either through hydrogen bonding (Thr 60, Gln159, Ser 180, Asn227, His308, Tyr309) or a salt bridge (Asp156 and Arg229). The conservation of many of these residues in the binding sites of other nucleotide sugar aminotransferases also suggests that they may be crucial for enzyme function (20,24). In order to explore whether these residues were indeed critical for catalysis, a panel of nine WbpE alanine mutants were generated using site-directed mutagenesis. In addition to eight residues identified above, a mutant in which the catalytic lysine (Lys185) was replaced with alanine was prepared as well. All mutants were purified as outlined above to high yield, and then tested for activity using the WbpB/WbpE coupled enzyme assay as previously described (15) (Figure S2, Supporting Information). As anticipated, the activity of the Lys185Ala mutant was completely abolished, but the other eight mutants exhibited nearly complete turnover of substrate to product under these reaction conditions, suggesting that the loss of binding affinity of any one of these residues may be compensated for by the cumulative efforts of the others. Individual reaction rates were not determined due to the difficulty in isolating the extremely labile ketone substrate of WbpE as well as the need for using the coupled WbpB/WbpE assay, which would mask the effect of a point mutation on the aminotransferase alone.

DISCUSSION

The glycosylation of proteins and lipids is a key post-translational modification common to all three kingdoms of life. These glycans serve to modulate the protein and lipid function in a vast number of ways, affecting processes such cellular signaling, protein folding, and the immune response. Despite the myriad cellular functions associated with these carbohydrates, the biosynthesis of monosaccharides in all organisms shares several common features, namely their activation as nucleotide sugars. In recent years, there has been a concerted effort to understand the biosynthetic machinery required for the elaboration of these conserved building blocks, particularly in bacteria, where they are found as part of natural products as well as components of the complex cell wall structures. To that end, we present the crystal structure of the UDP-GlcNAc(3keto)A aminotransferase WbpE from *P. aeruginosa* in complex with PMP, PLP, and the external aldimine of PLP with its aminated product. This study represents the first structure of an aminotransferase that binds a nucleotide sugar modified at the C2″, C3″ and C6″ positions. To date, there are three other known structures of Fold Type 1 aminotransferases bound to their nucleotide sugar substrates as the external aldimine (Figure 6). The first complex reported was that of PseC, an aminotransferase from *H. pylori* involved in the biosynthesis of pseudaminic acid (20). Shortly thereafter, the structures of both DesI, a key enzyme in the *S. venezuelae* desosamine

biosynthesis pathway, and QdtB, an aminotransferase required for synthesis of TDP-Qui*p*3NAc, were presented (22,24). Taken together, these structures provide an opportunity to gain a deeper understanding of the substrate specificity that governs the function of these enzymes.

A comparison of the active site orientations of the external aldimines in the four known structures (WbpE, PseC, DesI and QdtB) is presented in Figure 7. It can be seen that while the ligands are positioned quite differently within the binding sites depending primarily on the functional groups on the hexose rings, the structures do share some common features. As expected, the PLP cofactors are positioned in the same basic orientation. Also, each of the four hexose substrates contains a hydroxyl group at either the C3″ (QdtB and WbpE) or C4″ (PseC and DesI) position, and these hydroxyls are all situated on the same side of the active site near the catalytic lysine and the cofactor phosphate or an asparagine, in the case of DesI. Interestingly, all four hexoses seem to be bordered on the top and bottom faces by aromatic side chains, effectively sealing them off from the surrounding environment. One explanation for this observation is that association with these aromatic rings may serve to both stabilize the positively charged reaction intermediates through cation-π interactions and also prevent unwanted water molecules from entering into the active site and interfering with catalysis.

The many differences in nucleotide sugar orientation within the active site depicted in this analysis provide a glimpse into the requirements for substrate binding and specificity. In general, the hexose rings with smaller functional groups and less polarity are in contact with fewer atoms within the active site. This is rather unexpected, as often substrate binding causes conformational changes within the enzyme active site to create an induced fit. For example, while the nucleotide sugars bound to QdtB and WbpE are both anchored to the cofactor through the C3″ position, the QdtB ligand makes far fewer contacts to the active site atoms because of the smaller hexose modifications than the highly functionalized WbpE ligand. Similarly, the C6″ hexose carbons of the QdtB, PseC and WbpE ligands are all pointing in the same general direction, yet while there are no atoms within 4 Å of the QdtB and PseC C6″ methyl groups, the C6″ carboxylate of WbpE is coordinated to both the Arg229 in the β-hairpin domain as well as to a well-ordered water molecule. It is tempting to propose a relationship between increased space around the ligand hexose ring and decreased enzyme specificity. In their study of QdtB, Thoden, *et al* made a preliminary effort to address this theory by showing that QdtB accepts the C4″ epimer of its natural substrate, presumably due to the lack of protein contacts between the C4″ position of the hexose and the active site (24). However, further biochemical and biophysical studies are required to explore this hypothesis.

The WbpE structure complexed with its external aldimine intermediate described in this report provides the first example of a nucleotide sugar modified at the C6″ position within the enzyme active site. As alluded to previously, the C6″ carboxylate of the ligand is coordinated to Arg229 in the domain-swapped β-hairpin. This arginine residue is commonly found in Fold Type I aminotransferases, and has been shown to coordinate with the carboxylate of L-glutamate and α-KG in the first half of the reaction mechanism (18). Although there is as yet no direct evidence for where these two molecules bind within the WbpE active site, the crystal structure of a related aminotransferase ArnB was recently solved in complex with α-KG and clearly implicates this arginine in α-KG binding (19). Presuming that α-KG is present in the same location in WbpE as it is in ArnB, it can then be inferred that Arg229 of WbpE interacts with both enzyme substrates (L-glutamate and UDP-GlcNAc(3keto)A), playing a critical role in both halves of the catalytic cycle. This alignment of α-KG and the UDP-GlcNAc(3keto)A substrates within the active site of WbpE complements previous work in our laboratory on this pathway, in which we postulated that the unique NAD^+ cofactor regeneration exhibited by the dehydrogenase WbpB was

facilitated by the overlap of α-KG and UDP-GlcNAc(3keto)A within the substrate-binding pocket (15).

Another interesting feature of the WbpE structure is the presence of a non-prolyl *cis* amide bond between residues His308 and Tyr309 (Figure S3). The side chains of both of these residues line the active site of the protein and participate in important contacts with the nucleotide sugar to orient it properly. Studies of the prevalence of non-prolyl *cis* amide bonds within protein structures deposited in the Protein Data Bank indicate that they are extremely rare due to the increased steric strain between the neighboring Cα atoms. Interestingly, the location of these *cis* bonds is often found within functionally important regions of the protein. In addition, more than one-third of the characterized proteins containing *cis* amide bonds are present in carbohydrate-binding proteins (43). As depicted in Figures 5 and 7, both His308 and Tyr309 participate in key hydrogen bonds with the external aldimine intermediate, framing the upper region of the active site. However, it is clear that these residues are not absolutely crucial for catalysis, as our studies using alanine mutations at these positions still yielded functional enzyme (Figure S2). The close proximity of both His308 and Tyr309 to the hexose and pyrophosphate moieties held in place by the *cis* amide bond suggests that perhaps these residues impart specificity to the enzyme, effectively allowing only substrates of a certain shape to fit in the active site. Further biochemical analysis is required to explore this hypothesis, but difficulty in obtaining the ketone substrate of WbpE complicates these efforts.

While eukaryotes utilize only a limited set of carbohydrates as the basic building blocks for protein glycosylation, prokaryotes routinely incorporate a far greater number of sugar structures in order to maintain the sheer complexity and diversity of their glycans (44). Biochemical evidence has suggested that despite this structural diversity, diacetylated aminuronic acids such as ManNAc(3NAc)A are exceedingly rare. This class of highly functionalized sugars has primarily been identified in the complex cell wall matrices of a few pathogenic bacteria, such as *P. aeruginosa* and *B. pertussis*, as well as the flagellar glycoproteins of certain methanogenic archaea (45,46). However, an analysis of the rapidly growing database of newly sequenced prokaryotic genomes suggests that perhaps these aminuronic acids are more prevalent than previously suspected. A recent search for WbpE homologs resulted in over fifty matches with high sequence identity (> 40%); the eleven closest homologs are presented in Figure 8 and a full sequence alignment is provided in Figure S4. Interestingly, these homologs are all found in pathogenic bacteria, many of which have not been subject to in depth biochemical characterization. The presence of WbpE homologs in these organisms may imply that a ManNAc(3NAc)A-type carbohydrate exists in the cell wall matrix, where it could play a contributing role in modulating virulence and evasion of host defenses, though more work is required to characterize the cell wall components of these organisms to confirm their chemical makeup. Nevertheless, the protein structures reported in this study may offer insight into the biosynthetic enzymes in other pathogenic organisms and provide a unique opportunity for identification of important new targets for antibacterial drug development.

Supplementary Material

Refer to Web version on PubMed Central for supplementary material.

Acknowledgments

We are grateful to the staff at beamline X6A at the National Synchrotron Light Source, particularly Dr. Jean Jakoncic for assistance with data collection and analysis. Special thanks to Debby Pheasant of the Biophysical Instrumentation Facility at MIT for assistance with analytical centrifugation, Dr. Robert Grant of the Biology Department and members of the Drennan laboratory at MIT for technical advice, and colleagues in the Imperiali

laboratory, especially Dr. Matthieu Sainlos, Dr. Jerry Troutman and Meredith Hartley, for insight and helpful discussions.

References

1. Pier GB. *Pseudomonas aeruginosa* lipopolysaccharide: A major virulence factor, initiator of inflammation and target for effective immunity. Int J Med Microbiol. 2007; 297:277–295. [PubMed: 17466590]
2. Obritsch MD, Fish DN, MacLaren R, Rose J. Nosocomial infections due to multidrug-resistant *Pseudomonas aeruginosa*: epidemiology and treatment options. Pharmacotherapy. 2005; 25:1353–1364. [PubMed: 16185180]
3. Tang HB, DiMango E, Bryan R, Gambello M, Iglewski BH, Goldberg JB, Prince A. Contribution of specific *Pseudomonas aeruginosa* virulence factors to pathogenesis of pneumonia in a neonatal mouse model of infection. Infect Immun. 1996; 64:37–43. [PubMed: 8557368]
4. Diaz MH, Shaver CM, King JD, Musunuri S, Kazzaz JA, Hauser AR. *Pseudomonas aeruginosa* induces localized immunosuppression during pneumonia. Infect Immun. 2008; 76:4414–4421. [PubMed: 18663007]
5. Son MS, Matthews WJ Jr, Kang Y, Nguyen DT, Hoang TT. In vivo evidence of *Pseudomonas aeruginosa* nutrient acquisition and pathogenesis in the lungs of cystic fibrosis patients. Infect Immun. 2007; 75:5313–5324. [PubMed: 17724070]
6. Levy SB, Marshall B. Antibacterial resistance worldwide: causes, challenges and responses. Nat Med. 2004; 10:S122–S129. [PubMed: 15577930]
7. Mesaros N, Nordmann P, Plesiat P, Roussel-Delvallez M, Van Eldere JYG, Van Laethem Y, Jacobs F, Lebecque P, Malfroot A, Tulkens PM, Van Bambeke F. *Pseudomonas aeruginosa*: resistance and therapeutic options at the turn of the new millennium. Clin Microbiol Infect. 2007; 13:560–578. [PubMed: 17266725]
8. Hancock RE. Resistance mechanisms in *Pseudomonas aeruginosa* and other nonfermative gram-negative bacteria. Clin Infect Dis. 1998; 27:S93–S99. [PubMed: 9710677]
9. Cryz SJ Jr, Pitt TL, Furer E, Germanier R. Role of lipopolysaccharide in virulence of *Pseudomonas aeruginosa*. Infect Immun. 1984; 44:508–513. [PubMed: 6425224]
10. Hancock RE, Mutharia LM, Chan L, Darveau RP, Speert DP, Pier GB. *Pseudomonas aeruginosa* isolates from patients with cystic fibrosis: a class of serum-sensitive, nontypable strains deficient in lipopolysaccharide O side chains. Infect Immun. 1983; 42:170–177. [PubMed: 6413410]
11. Engels W, Endert J, Kamps MA, van Boven CP. Role of lipopolysaccharide in opsonization and phagocytosis of *Pseudomonas aeruginosa*. Infect Immun. 1985; 49:182–189. [PubMed: 3924827]
12. Dasgupta T, de Kievit TR, Masoud H, Altman E, Richards JC, Sadovskaya I, Speert DP, Lam JS. Characterization of lipopolysaccharide-deficient mutants of *Pseudomonas aeruginosa* derived from serotypes O3, O5, and O6. Infect Immun. 1994; 62:809–817. [PubMed: 8112851]
13. Kochetkov NK, Knirel YA. Structure of lipopolysaccharides from gram-negative bacteria. III Structure of O-specific polysaccharides. Biochemistry (Moscow). 1994; 59:1325–1383.
14. Rocchetta HL, Burrows LL, Lam JS. Genetics of O-antigen biosynthesis in *Pseudomonas aeruginosa*. Microbiol Mol Biol Rev. 1999; 63:523–553. [PubMed: 10477307]
15. Larkin A, Imperiali B. Biosynthesis of UDP-GlcNAc(3NAc)A by WbpB, WbpE, and WbpD: Enzymes in the Wbp Pathway Responsible for O-Antigen Assembly in *Pseudomonas aeruginosa* PAO1. Biochemistry. 2009; 48:5446–5455. [PubMed: 19348502]
16. Burrows LL, Charter DF, Lam JS. Molecular characterization of the *Pseudomonas aeruginosa* serotype O5 (PAO1) B-band lipopolysaccharide gene cluster. Mol Microbiol. 1996; 22:481–495. [PubMed: 8939432]
17. John RA. Pyridoxal phosphare-dependent enzymes. Biochim Biophys Acta. 1995; 1248:81–96. [PubMed: 7748903]
18. Eliot AC, Kirsch JF. Pyridoxal Phosphate Enzymes: Mechanistic, Structural, and Evolutionary Considerations. Annu Rev Biochem. 2004; 73:383–415. [PubMed: 15189147]
19. Noland BW, Newman JM, Hendle J, Badger J, Christopher JA, Tresser J, Rutter ME, Sanderson WE, Müller-Dieckmann H-J, Gajiwala KS, Buchanan SG. Structural Studies of *Salmonella*

typhimurium ArnB (PmrH) Aminotransferase: A 4-Amino-4-Deoxy-L-Arabinose Lipopolysaccharide-Modifying Enzyme. Structure (London, England : 1993). 2002; 10:1569–1580.

20. Schoenhofen IC, Lunin VV, Julien JP, Li Y, Ajamian E, Matte A, Cygler M, Brisson JR, Aubry A, Logan SM, Bhatia S, Wakarchuk WW, Young NM. Structural and Functional Characterization of PseC, an Aminotransferase Involved in the Biosynthesis of Pseudaminic Acid, an Essential Flagellar Modification in *Helicobacter pylori*. J Biol Chem. 2006; 281:8907–8916. [PubMed: 16421095]
21. Burgie ES, Thoden JB, Holden HM. Molecular architecture of DesV from *Streptomyces venezuela*e: A PLP-dependent transaminase involved in the biosynthesis of the unusual sugar desosamine. Protein Sci. 2007; 16:887–896. [PubMed: 17456741]
22. Burgie ES, Holden HM. Molecular Architecture of DesI: A Key Enzyme in the Biosynthesis of Desosamine. Biochemistry. 2007; 46:8999–9006. [PubMed: 17630700]
23. Cook PD, Holden HM. GDP-Perosamine Synthase: Structural Analysis and Production of a Novel Trideoxysugar. Biochemistry. 2008; 47:2833–2840. [PubMed: 18247575]
24. Thoden JB, Schäffer C, Messner P, Holden HM. Structural Analysis of QdtB, an Aminotransferase Required for the Biosynthesis of dTDP-3-acetamido-3,6-dideoxy-a-D-glucose. Biochemistry. 2009; 48:1553–1561. [PubMed: 19178182]
25. Van Duyne GD, Standaert RF, Karplus PA, Schreiber SL, Clardy J. Atomic Structures of the Human Immunophilin FKBP-12 Complexes with FK506 and Rapamycin. J Mol Biol. 1993; 29:105–124. [PubMed: 7678431]
26. Stafford WF, Sherwood PJ. Analysis of heterologous interacting systems by sedimentation velocity: curve fitting algorithms for estimation of sedimentation coefficients, equilibrium and kinetic constants. Biophys Chem. 2004; 108:231–243. [PubMed: 15043932]
27. Otwinowski Z, Minor W. Processing of X-ray Diffraction Data Collected in Oscillation Mode. Methods in Enzymology. 1997; 276:307–326.
28. Collaborative Computational Project. The CCP4 Suite: Programs for Protein Crystallography. Acta Crystallogr, Sect D: Biol Crystallogr. 1994; D50:760–763.
29. Hendrickson WA. Determination of macromolecular structures from anomalous diffraction of synchrotron radiation. Science. 1991; 254:51–58. [PubMed: 1925561]
30. Terwilliger TC, Berendzen J. Automated MAD and MIR structure solution. Acta Crystallogr, Sect D: Biol Crystallogr. 1999; D55:849–861. [PubMed: 10089316]
31. Terwilliger TC. Automated main-chain model building by template matching and iterative fragment extension. Acta Crystallogr Sect D: Biol Crystallogr. 2003; 59:38–44. [PubMed: 12499537]
32. Terwilliger TC. Maximum-likelihood density modification. Acta Crystallogr Sect D: Biol Crystallogr. 2000; 56:965–972. [PubMed: 10944333]
33. Storoni LC, McCoy AJ, Read RJ. Likelihood-enhanced fast rotation functions. Acta Crystallogr, Sect D: Biol Crystallogr. 2004; D60:432–438. [PubMed: 14993666]
34. Emsley P, Cowtan K. Coot: model-building tools for molecular graphics. Acta Crystallogr, Sect D: Biol Crystallogr. 2004; D60:2126–2132. [PubMed: 15572765]
35. Murshudov GN, Vagin AA, Dodson EJ. Refinement of Macromolecular Structures by the Maximum-Likelihood Method. Acta Crystallogr, Sect D: Biol Crystallogr. 1997; D53:240–255. [PubMed: 15299926]
36. Brünger AT. Assessment of Phase Accuracy by Cross Validation: the Free *R* Value, Methods and Applications. Acta Crystallogr, Sect D: Biol Crystallogr. 1993; D49:24–36.
37. Lamzin, VS.; Perrakis, A.; Wilson, KS. The ARP/wARP suite for automated construction and refinement of protein models. In: Rossmann, MG.; Arnold, E., editors. Int Tables for Crystallography. Kluwer Academic Publishers; Dordrecht: 2001. p. 720-722.
38. Laskowski RA, MacArthur MW, Moss DS, Thornton JM. PROCHECK: a program to check the stereochemical quality of protein structures. J Appl Cryst. 1993; 26:283–291.
39. Vaguine AA, Richelle J, Wodak SJ. SFCHECK: a unified set of procedures for evaluating the quality of macromolecular structure-factor data and their agreement with the atomic model. Acta Crystallogr, Sect D: Biol Crystallogr. 1998; D55:191–205.

40. Davis IW, Leaver-Fay A, Chen VB, Block JN, Kapral GJ, Wang GJ, Wang X, Murray LW, Arendal B III, Snoeyink J, Richardson JS, Richardson DC. MolProbity: all-atom contacts and structure validation for proteins and nucleic acids. Nucleic Acids Res. 2007; 35:W375–W383. [PubMed: 17452350]

41. Ford GC, Eichele G, Jansonius JN. Three-dimensional structure of a pyridoxal-phosphate-dependent enzyme, mitochondrial aspartate aminotransferase. Proc Natl Acad Sci USA. 1980; 77:1559–2563.

42. Jansonius JN. Structure, evolution and action of vitamin B_6-dependent enzymes. Curr Opin Struct Biol. 1998; 8:759–769. [PubMed: 9914259]

43. Jabs A, Weiss M, Hilgenfeld. Non-proline Cis peptide bonds in proteins. J Mol Biol. 1999; 286:291–304. [PubMed: 9931267]

44. Varki, A.; Cummings, RD.; Freeze, HH.; Stanley, P.; Bertozzi, CR.; Hart, GW.; Etzler, ME. Essentials of Glycobiology. 2. Cold Spring Harbor Laboratory Press; New York: 2008.

45. Kelly J, Logan SM, Jarrell KF, VanDyke DJ, Vinogradov EV. A novel *N*-linked flagellar glycan from *Methanococcus maripalidus*. Carb Res. 2009; 344:648–653.

46. Caroff M, Brisson J-R, Martin A, Karibian D. Structure of the *Bordetella pertussis* 1414 endotoxin. FEBS Lett. 2000; 477:8–14. [PubMed: 10899302]

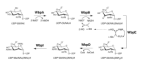

Figure 1.
Biosynthetic pathway of UDP-ManNAc(3NAc)A in *P. aeruginosa* PAO1 (serotype O5). Abbreviations: AcCoA, acetyl-coenzyme A; CoA, coenzyme A; 2-HG, 2-hydroxyglutarate; α-KG, α-ketoglutarate; NAD^+, nicotinamide adenine dinucleotide; NADH, nicotinamide adenine dinucleotide (reduced); PLP, pyridoxal 5′-phosphate; PMP, pyridoxamine 5′-phosphate.

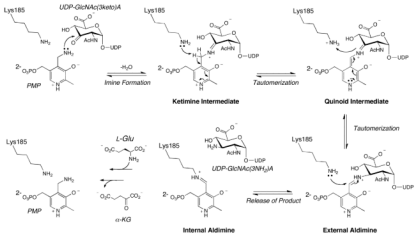

Figure 2.
Proposed reaction mechanism of WbpE.

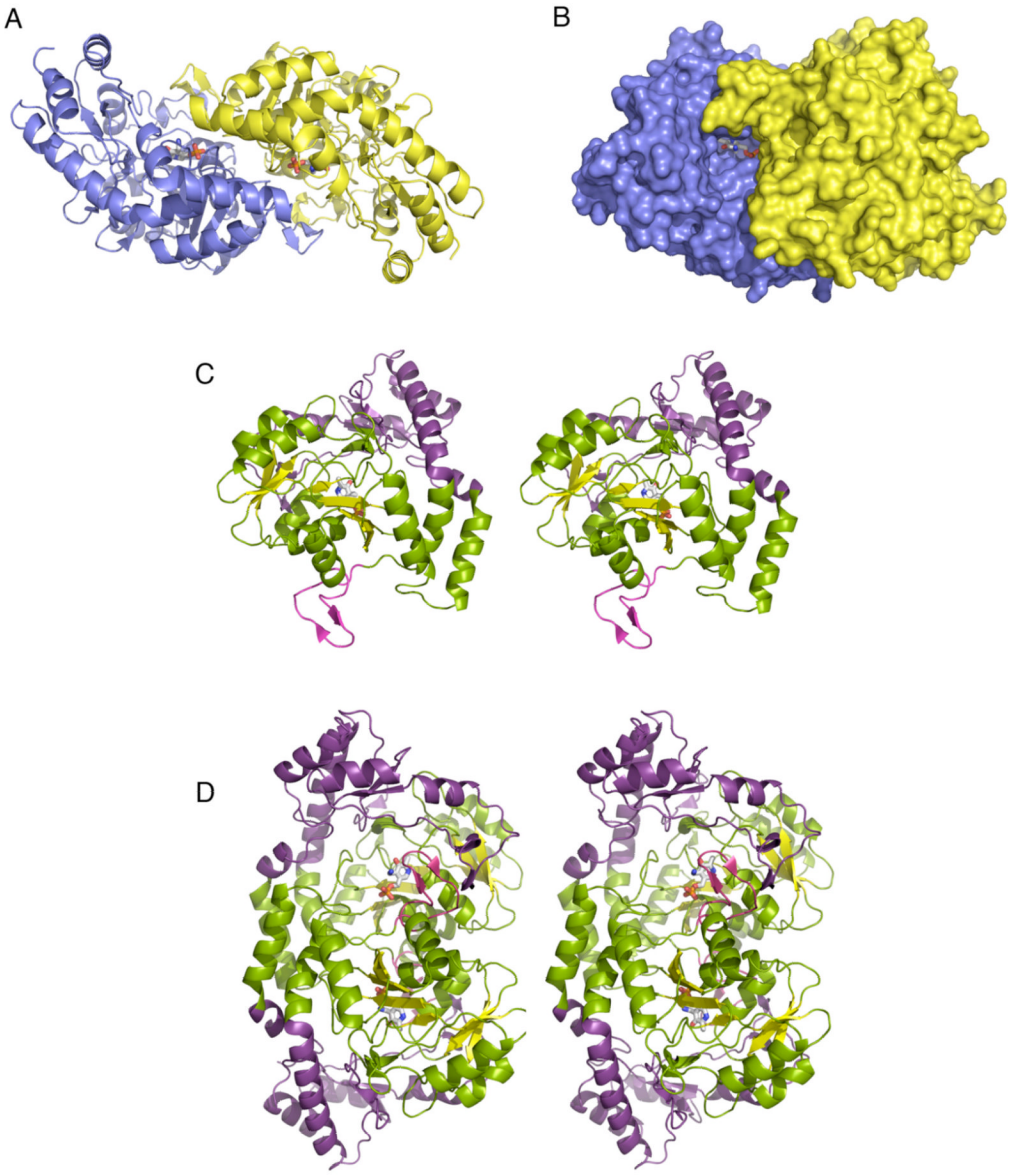

Figure 3.
Crystal structure of the WbpE-PMP complex. A) Structure of the homodimer, with each subunit colored individually and the PLP cofactor shown as sticks; B) Space-filling model of the homodimer, where the PMP cofactor can be observed at the end of the deep cavity; C) Stereo diagram of a single subunit, with the N- and C-terminal domains colored green and purple, respectively. The β-strands comprising the central β-sheet are highlighted in yellow, and the domain-swapped β-hairpin is shown in magenta; D) Stereo diagram of the homodimer, with the various domain features colored as described in C.

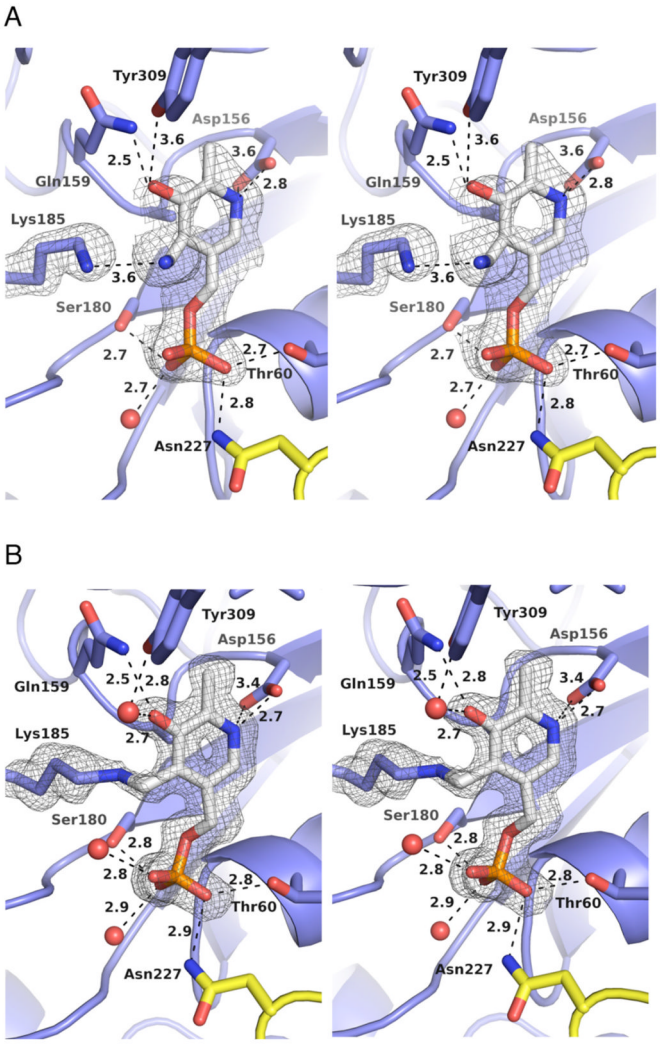

Figure 4.

Close-up view of the cofactor binding site. The 2(F_o-F_c) electron density maps are contoured at 3σ for both the PMP-bound (A) and PLP-bound (B) structures, and were calculated with atoms of the cofactor and Lys185 side chain omitted. Amino acids corresponding to subunits 1 and 2 are shown in blue and yellow, respectively, and water molecules are depicted as red spheres. All interactions within a 3.6 Å distance of the cofactor are indicated by dashed lines except for those that line the top face of the cofactor binding site; these residues were removed from the figure for clarity but are outlined in the text.

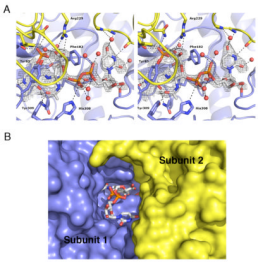

Figure 5.

Close-up view of the external aldimine-bound structure. A) The external aldimine of PLP and UDP-GlcNAc(3NH_2)A in the active site of WbpE. The 2(F_o-F_c) electron density map is contoured at 1.5σ, and was calculated with atoms of the external aldimine omitted. Residues within a 4 Å radius of the ligand are indicated and water molecules are depicted as red spheres. B) A space-filling model of the WbpE external aldimine complex, highlighting the manner in which the uridine moiety extends up through the deep cavity to the solvent. In both figures, the subunits of the dimer are depicted in blue and yellow.

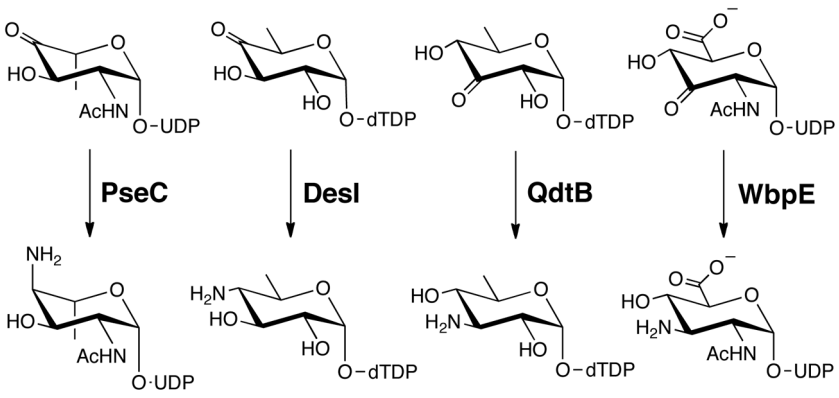

Figure 6.

The reactions carried out by homologous nucleotide sugar aminotransferases PseC, DesI, QdtB and WbpE. All reactions require the PLP and concomitant conversion of L-glutamate to α-ketoglutarate.

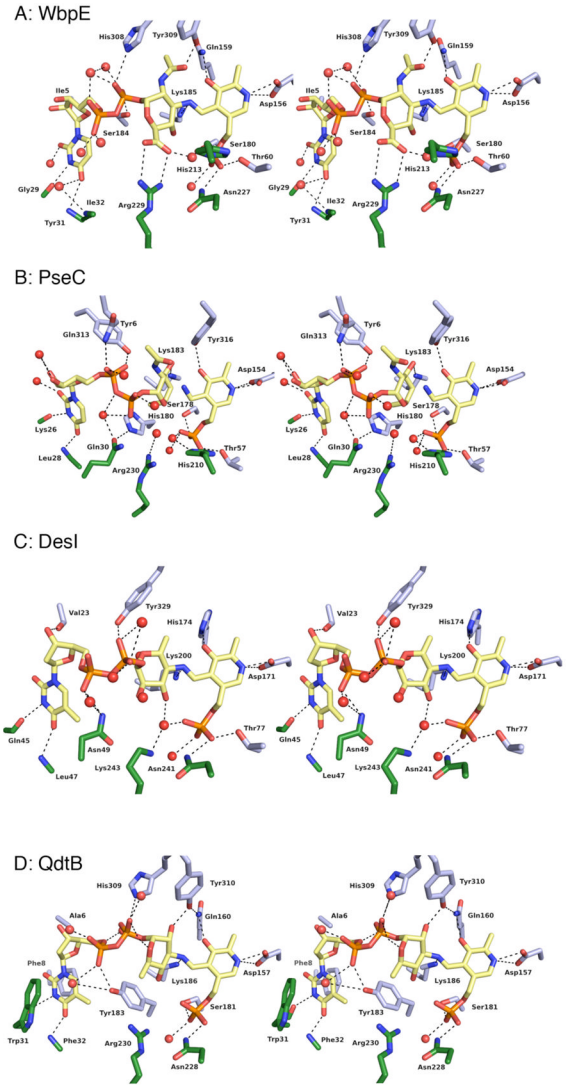

Figure 7.

Comparison of the structures of WbpE (A), PseC (B), DesI (C) and QdtB (D) in complex with the corresponding external aldimines. For each structure, subunit 1 is colored gray and the domain-swapped enzymes from the neighboring subunit are shown in green. Interactions within a 3.6 Å distance of the ligand are shown as black lines, and residues lining the top face of the enzyme were removed for clarity. All four complexes are positioned with the PLP cofactor in the same orientation in order to highlight the differences in ligand conformation in each active site. In addition, the basic residue in each enzyme important for α-KG binding (Arg or Lys) is specifically labeled.

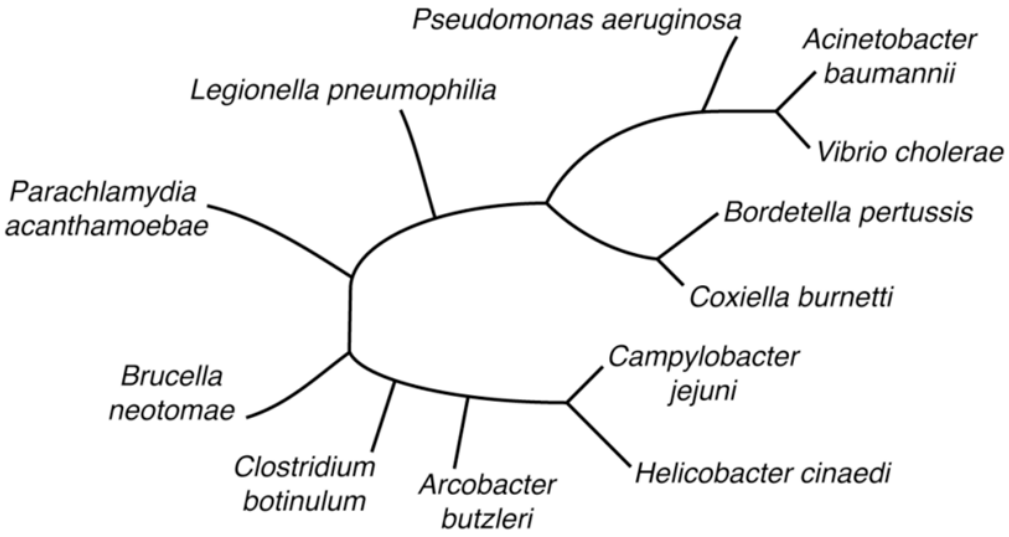

Figure 8.
A phylogenetic tree indicating homologs of WbpE from pathogenic bacteria. Each homolog indicated has a sequence identity > 40% to WbpE. A full sequence alignment is depicted in Figure S4.

Table 1

Data Collection and Refinement Statistics

	PMP	PLP	External Aldimine	SeMet[a]
Data Collection				
Space group	$P2_12_12$	$P2_12_12$	$P2_12_12$	$P2_12_12$
Unit cell dimensions (*a*, *b*, *c*) (Å)	78.28, 149.29, 54.90	77.79, 148.72, 53.22	78.29, 149.67, 55.12	77.81, 149.03, 53.29
Resolution (Å)	50.0-1.95	20.0-1.50	20.0-1.83	50.0-1.93
Observed reflections	45,308	94,182	46,379	46,078
R_{merge} (%)[b,c]	7.3(42.0)	9.1(66.2)	7.1(49.2)	8.2(41.9)
$I/\sigma I$[c]	53.4(9.2)	35.8(3.0)	36.3(4.1)	36.7(5.8)
Completeness (%)[c]	99.8	99.7	98.6	100
Redundancy[c]	14.6(14.5)	7.9(7.0)	7.3(6.7)	7.5 (7.2)
Refinement				
Resolution (Å)	35–1.95	20–1.50	20–1.90	
R_{work}/R_{free} (%)[d,e]	19.8/24.6	17.9/22.2	18.7/24.5	
Total Number of Atoms	5837	5880	6027	
Protein	5428	5471	5401	
Water	377	409	516	
Ligands	32	32	110	
B-factors (Å^2)				
Overall	28.2	20.5	19.8	
Protein	28.3	19.1	19.3	
Water	29.4	22.7	27.4	
Ligand	15.0	16.9	34.8	
Ramachandram plot (%)[f]	96.8/2.8/0.4	97.1/2.7/0.3	96.0/3.8/0.3	
r.m.s. deviations				
Bond lengths (Å)	0.010	0.011	0.016	
Bond angles (°)	1.245	1.250	1.350	
PDB code	xxx	xxx	xxx	

[a] Data reported for the SeMet derivative refer to those collected at the selenium peak wavelength.

[b] The number in parathenses represents the highest resolution bin; 1.98-1.94, 1.55-1.5, 1.86-1.83 and 2.01-1.93 Å, for the data sets of PMP, PLP, external aldimine and the SeMet derivative, respectively.

[c] $R_{merge} = \Sigma||I-<I>|/\Sigma I$, where I is the intensity of a reflection, and $<I>$ is the mean intensity of group of equivalent reflections.

[d] $R_{work} = \Sigma h\, ||F(h)_{obs}|-|F(h)_{calc}||/\Sigma h|F(h)_{obs}|$

[e] R_{free} was calculated for 5% of the reflections randomly excluded from the refinement.

[f] Ramachandran plot statistics are given as core/allowed/generously allowed and are for both chains.